Available online at www.sciencedirect.com
ScienceDirect
Acta Materialia 59 (2011) 5250–5256
Acta MATERIALIA
www.elsevier.com/locate/actamat

Validating computed grain boundary energies in fcc metals using the grain boundary character distribution

Elizabeth A. Holm [a,*], Gregory S. Rohrer [b], Stephen M. Foiles [a], Anthony D. Rollett [b], Herbert M. Miller [b], David L. Olmsted [c]

[a] Computational Materials Science and Engineering Department, Sandia National Laboratories, Albuquerque, NM 87185-1411, USA
[b] Department of Materials Science and Engineering, Carnegie Mellon University, Pittsburgh, PA 15213-3890, USA
[c] Department of Materials Science and Engineering, University of California, Berkeley, CA 94720, USA

Received 30 March 2011; received in revised form 2 May 2011; accepted 3 May 2011
Available online 12 June 2011

Abstract

The grain boundary character distribution (GBCD) is a direct measurement that can be determined from a single planar section. Since the GBCD is inversely related to the grain boundary energy distribution, it offers a useful metric for validating grain boundary energy calculations. Comparisons between the measured GBCD and calculated energies for 388 grain boundaries in Al show that, for boundaries with a statistically reliable number of observations, including general, Σ3, Σ7, Σ11 and ⟨1 1 1⟩ twist boundaries, the GBCD and calculated grain boundary energy have weighted correlation coefficients of approximately 0.9, reproducing both qualitative and quantitative trends seen in simulations. GBCDs for Ni and Al are positively correlated, as predicted by simulation. By combining GBCD measurements with simulation results, we validate grain boundary energy simulations in both low and high stacking fault energy metals.

Keywords: Grain boundary energy; Grain boundary character; MD simulations; EBSD

1. Introduction

Validation poses a significant challenge for computer simulations of grain boundary properties, such as those reviewed in Refs. [1–6]. Because properties such as grain boundary energy are difficult to measure, experimental data is sparse, and is often available only for a few particular grain boundaries in a given material [7–21]. New, high-throughput techniques based on microstructural analysis have changed this situation [22–32]. For example, a recent comparison between 388 measured and calculated grain boundary energies in Ni showed excellent agreement for high population boundary types [33].

Because Ni has a moderate stacking fault energy, twins dominate the experimental Ni microstructures; all the high population boundaries were of the Σ3 or Σ9 types. Other boundaries were present in much lower numbers, and poor statistics prevented a comparison between experiment and simulation for these boundaries.

In analyzing the energy comparison in Ni, we suggested that a high stacking fault energy material would not be dominated by twinning, and would instead have a more uniform distribution of grain boundary types [33]. Analyzing such a microstructure could permit grain boundary energy comparisons for additional boundaries beyond the Σ3 and Σ9 types. In this paper, we compare experimental results with computed grain boundary energies for a variety of boundary types in Al, a high stacking fault energy material. We find excellent agreement between measurements of grain boundary populations and computed grain boundary energies for high population boundaries, including boundary types that had not been validated previously, such as Σ7 and ⟨1 1 1⟩ twist boundaries.

* Corresponding author.
E-mail address: Eaholm@sandia.gov (E.A. Holm).

1359-6454/$36.00
doi:10.1016/j.actamat.2011.05.001

2. Method

2.1. Computational calculations of grain boundary energy

The computational method for constructing a large catalog of grain boundaries and calculating their energies has been described in detail previously [6]. In this paper, we utilize energy data from a catalog of 388 Al grain boundaries, which includes all the boundaries that can be constructed within a periodic cell of maximum size $15a_0/2$, where a_0 is the lattice parameter. For each boundary, several hundred to several thousand candidate structures are constructed via systematic perturbations of the microscopic degrees of freedom. The $T = 0$ K energy (i.e. the enthalpy) of each structure is minimized using molecular statics, and the lowest energy structure is presumed to be the equilibrium structure.

The material model for Al in these calculations is an embedded atom method potential [34], parameterized by Ercolessi and Adams to represent Al [35]. This potential reproduces planar defects, such as the stacking fault energy and low index surface energies, with reasonable fidelity, although the values are uniformly somewhat low. Other sources of error in these calculations are discussed in detail in Ref. [33]. The complete data set of Al grain boundary geometries and energies is publicly available as online supplemental material to Ref. [6].

2.2. Experimental grain boundary energy measurements

The method for measuring relative grain boundary energies in polycrystals has been described in detail previously [26–28,30–32]. The first step involves measuring the grain boundary character distribution (GBCD), which is the population distribution of boundary types. For each grain boundary, electron backscatter diffraction microscopy is used to determine four of the five macroscopic degrees of freedom of the boundary crystallography as well as the boundary area [28,32]; the fifth degree of freedom is derived from stereological analysis of boundary traces as described in Ref. [30]. Since grain boundaries that are close in crystallography are generally similar in energy, boundaries are binned in the five-dimensional crystallographic space, with a bin width given by a generalized Brandon criterion [36]; this procedure accounts for crystallographic symmetries and multiplicities [28].

The binned data corresponds to the area-weighted GBCD. Triple junction angle information, measured from reconstructed serial sections, can be combined with the GBCD and optimized to produce the grain boundary energy distribution (GBED) [22,31]; however, in this paper we shall consider only the GBCD, as discussed below.

For this study, we used the GBCD data measured for an Al polycrystal of commercially pure alloy 1050. The sample processing and orientation mapping was carried out as described in Ref. [29]. The analysis resulted in 77,000 distinct grain boundary line segments. Boundaries were binned into equal volume bins spanning approximately 10° in each of the five macroscopic degrees of freedom, yielding 6521 distinct grain boundary types. Only the 388 grain boundary types included in the computer simulations are considered here. The population of each boundary type is expressed in units of multiples of a random distribution (MRD), where a boundary type with population x MRD would be present at x times the expected population in a random distribution of grain boundaries. In this data set, a population of 1 MRD corresponds to approximately 12 grain boundaries (assuming equal grain boundary lengths).

To compare the simulated boundaries to the experimental data, we extract the rotation angle and axis and boundary plane for each and apply all possible face-centered cubic (fcc) symmetry operators. For each equivalent boundary, we identify the appropriate grain boundary type (i.e. bin) in the experimental system and read the population from the GBCD. The average population for all the equivalent boundaries is taken as the relevant experimental population, to be compared to the calculated energy value.

2.3. The relationship between the GBCD and the GBED

Derived from crystallographic and geometric measurements, the GBCD gives an area-weighted population for each grain boundary type. If the Herring relation is obeyed (i.e. triple junctions are in local equilibrium), the GBCD data can be combined with triple junction angle measurements to give a system of equations that can be solved for the relative GBED. However, both the measurement of triple junction angles via serial section reconstruction and the solution of the system of equations via numeric optimization introduce sources of error [33]. Thus, the GBCD is the more direct and accurate representation of the microstructure.

Because grain boundary evolution is driven by grain boundary energy, it is not surprising that the GBCD is related to the GBED. Both theory and experiments show that the GBCD is inversely related to the GBED, such that $\ln(P) \propto \gamma$, where P is the boundary population in units of MRD and γ is the grain boundary free energy [25,28,33,37–39]. In our previous comparison between measured and calculated grain boundary energies in Ni, we found that the GBCD, expressed as $\ln(P)$, was more strongly correlated with the calculated grain boundary energy than the GBED was; furthermore, the GBCD had fewer spurious data points [33]. Therefore, in this paper, we use the experimental GBCD to compare with the computed energies for Al grain boundaries.

3. Results and discussion

3.1. All boundaries

Fig. 1 shows the relationship between the experimental GBCD and the computed grain boundary energy, expressed as $\ln(P)$ vs. γ, for the 388 simulated Al grain

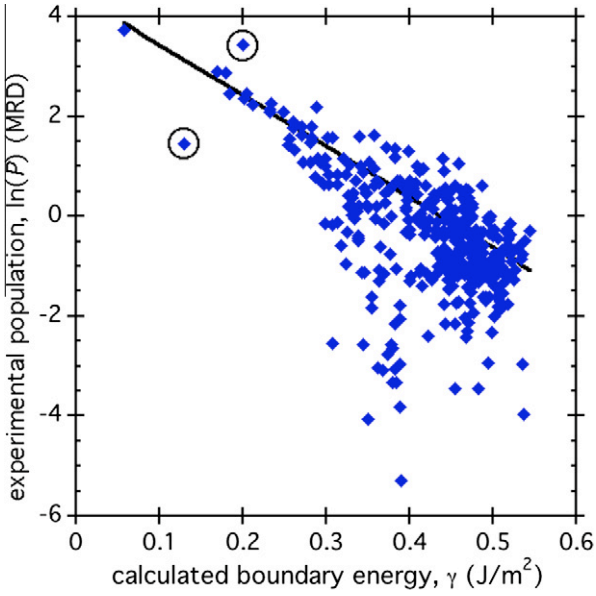

Fig. 1. The relationship between experimental GBCD and calculated grain boundary energy for 388 grain boundaries in Al. The data are represented well by a linear curve fit, weighted by population (solid line). Two outliers (circled) are described in the text.

boundaries. There is a clear inverse correlation, with the scatter increasing as P decreases. However, a standard least-squares fit of the data gives a poor fit with a modest unweighted correlation coefficient, $R_U = 0.57$. In our previous study on Ni, we found that the agreement between experiment and computation improved as the experimental observation frequency increased. Therefore, we weighted the experimental measurements by P using the locally weighted least-squares error method when calculating curve fits [33]. If we perform a population-weighted fit in Fig. 1, we find excellent correlation between the measured GBCD and the computed grain boundary energy (weighted correlation coefficient $R_W = 0.91$), and the resulting line appears to be a reasonable representation of the data.

Interestingly, there are two significant outliers in the experimental GBCD data, circled in Fig. 1. The 50.6° [1 1 1](1 1 1) symmetric twist boundary appears at a higher P than suggested by its energy. This is an artifact of the discretization used to calculate the GBCD. Because the separation between this boundary and the Σ3 boundary is less than the average bin width, some of the more common Σ3 boundaries contribute to this bin and lead to an overestimation. As a test, if we move this bin more than a bin width away from the Σ3 to 49°[1 1 1](1 1 1), the population decreases to $P = 8.3$ MRD, which is consistent with the trend line in Fig. 1. The distance between the 49°[1 1 1](1 1 1) boundary and the 50.6°[1 1 1](1 1 1) boundary is small compared to the bin width, so we would expect a high population of 50.6° boundaries to increase the observed population of 49° boundaries. That this does not occur confirms that the 50.6° boundary itself is not a high population type; its high P is an artifact of its proximity to the Σ3 boundary.

The Σ11 50.5°[1 1 0](3 1 1) symmetric tilt boundary appears at lower P than suggested by its energy. This boundary has been calculated and observed to have especially low energy [6,13], and in the molecular dynamics (MD) survey of grain boundary energies it was found to have an anomalously low energy in Al compared to other fcc metals [6,40]. While it is possible that the calculated energy is spurious, the most likely simulation error is to examine an incorrect (i.e. non-minimal energy) boundary structure, which yields a boundary energy that is too high, rather than too low. The experimental analysis will tend to underestimate the population of boundaries that represent sharp cusps in energy. However, in that case, increasing the resolution of the discretization should increase the observed population; that does not occur for this boundary. As discussed below, it is possible that the Σ11 boundaries may follow a different scaling between ln(P) and γ, but why Σ11 boundaries should scale differently is not clear. At this point, the anomalously low population of Σ11 50.5°[1 1 0](3 1 1) boundaries has not been convincingly explained.

The boundary population range in Al is much narrower than in Ni, and the Al GBCD is much flatter than the Ni GBCD, even when adjusted for the differences in binning (discussed below). While the Ni data forms distinct population clusters, the Al data does not indicate separate population groups. However, we can divide the Al data into relatively high P boundaries ($P \geqslant 1$ MRD, 12 or more measurements per bin), shown in Fig. 2a, and low P boundaries ($P < 1$ MRD, fewer than 12 measurements per bin), shown in Fig. 2b. The high P boundaries show excellent unweighted and weighted correlations between ln(P) and γ ($R_U = 0.79$; $R_W = 0.90$). For these boundaries, the measured GBCD gives a good estimate of the relative grain boundary energy and convincingly validates the simulation results. The low P boundaries show almost no correlation ($R_U = 0.12$; $R_W = 0.13$) with substantial scatter. For these infrequently observed boundary types, simulations give a better estimate of grain boundary energy than can be deduced from the GBCD.

It is worth noting that in Al the number of boundaries required for statistical confidence (12 or more measurements per bin) is similar to that previously found in Ni (13 or more measurements per bin) [33]. However, because twinning does not interfere with the development of the general boundary network in Al, more Al boundary types achieve statistical significance, allowing more opportunities for comparisons with simulated boundaries.

3.2. Σ3 boundaries

Despite aluminum's high stacking fault energy, the most prevalent boundaries are of the Σ3 type. The coherent twin is the highest population boundary type ($P = 42$ MRD), and seven of the most populous ten boundary types are Σ3 boundaries. However, some Σ3 boundary types are present in very low numbers. The wide range of Σ3 bound-

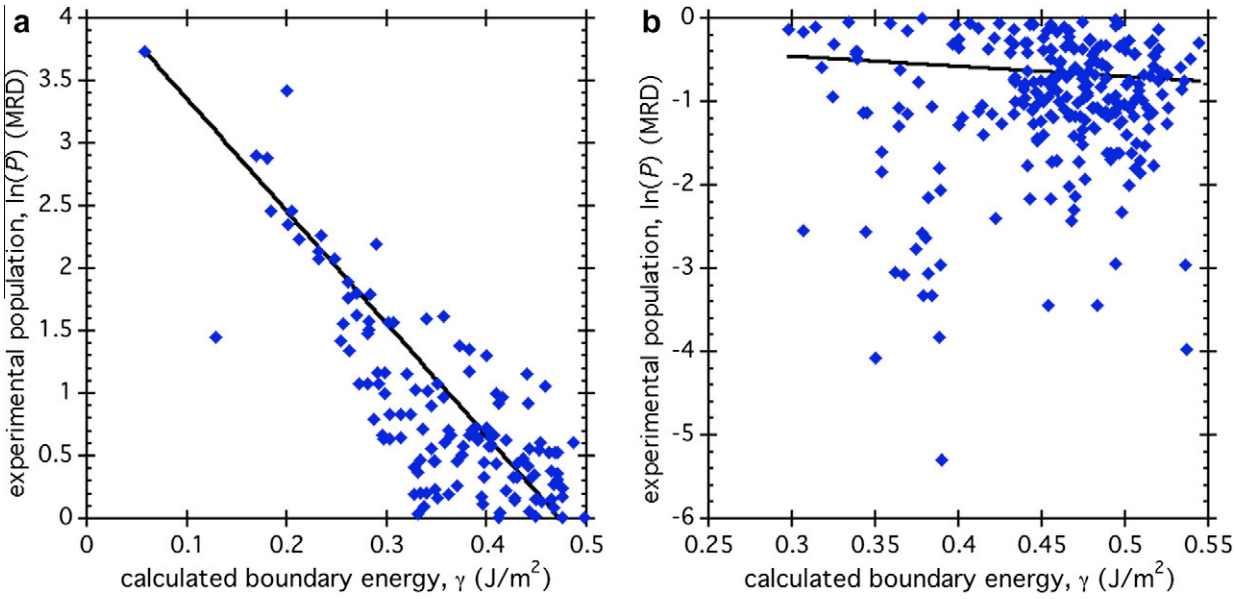

Fig. 2. The relationship between experimental GBCD and calculated grain boundary energy in Al for (a) high population boundary types with $P \geqslant 1$ MRD and (b) low population boundary types with $P < 1$ MRD. Population-weighted linear fits are shown as solid lines. The correlation is excellent for high P boundaries and minimal for low P boundaries.

ary populations indicates a wide range in Σ3 boundary energies for fcc metals, as confirmed by simulations [6,41]. For Σ3 boundaries, the measured GBCD scales well with the calculated energy for high population boundaries ($P > 1$), with substantial scatter for low population boundaries, as shown in Fig. 3a; the weighted correlation is excellent ($R_W = 0.92$).

Although Σ3 boundaries are widely observed in Al, they are much more prevalent in Ni, which has a lower stacking fault energy and is highly twinned. In Ni, the 41 Σ3 boundaries we examined were the highest population boundaries; none were of moderate or low population; and together they comprised 40% of all boundaries observed. Furthermore, Σ9 boundaries, which form at the intersection of two Σ3 boundaries, are also abundant in Ni but are scarcely seen in Al. Finally, in Ni, Σ3 and Σ9 boundaries form distinct population clusters that scale differently with energy than general boundaries [33], indicating that the Σ3 and Σ9 boundaries form a discrete twin boundary subnetwork within the microstructure; in Al, Σ3 and Σ9 boundary populations are integrated into the general GBCD, suggesting they do no form a twin boundary subnetwork. Together, these observations suggest that twinning is not a dominant microstructural evolution mechanism in Al, in agreement with predictions based on stacking fault energy.

3.3. Other CSL boundaries

Σ7 boundaries are known to be important in Al (cf. [42,43]). While Σ7 boundaries are minimally observed in Ni, they are quite prevalent in Al. As shown in Fig. 3b, the Σ7 GBCD correlates well with calculated grain boundary energies over the range of observed populations ($R_U = 0.91$; $R_W = 0.92$).

Σ11 boundaries are also more plentiful in Al than in Ni. They show good weighted correlation between measured GBCD and calculated energy ($R_W = 0.93$), as shown in Fig. 3c. It is interesting to note that the slopes of the lines generated by a weighted linear fit of ln(P) vs. γ are within the range $-12 \leqslant m \leqslant -9$ for all the boundary types examined, with the exception of the Σ11 boundaries, where $m = -7$. This suggests that Σ11 boundaries may form a separate cluster in GBCD space, as previously observed for Σ3 and Σ9 boundaries in Ni [33]. This might also explain why the population of the low-energy Σ11 50.5°[1 1 0](3 1 1) boundary does not follow the same scaling with energy as the other boundaries in the system. However, why the Σ11 boundaries should scale differently from other boundary types is not clear.

Σ5, Σ9 and Σ15 boundaries are scarce in Al. Their low populations cause large scatter in the GBCD and poor correlation with calculated energies; for these boundaries, we would expect simulation to give a better estimate of energy than the measured GBCD provides.

3.4. ⟨1 1 1⟩ twist boundaries

Measurements of the Al GBCD indicate a preference for grain boundaries that contain at least one ⟨1 1 1⟩ plane [29]. Although the computational survey did not include any boundaries with a single ⟨1 1 1⟩ plane, it does examine a series of ⟨1 1 1⟩ symmetric twist boundaries, which are all of low energy. These boundaries are of uniformly high population in Al, and they show excellent correlation between the measured GBCD and the calculated energy ($R_U = 0.90$;

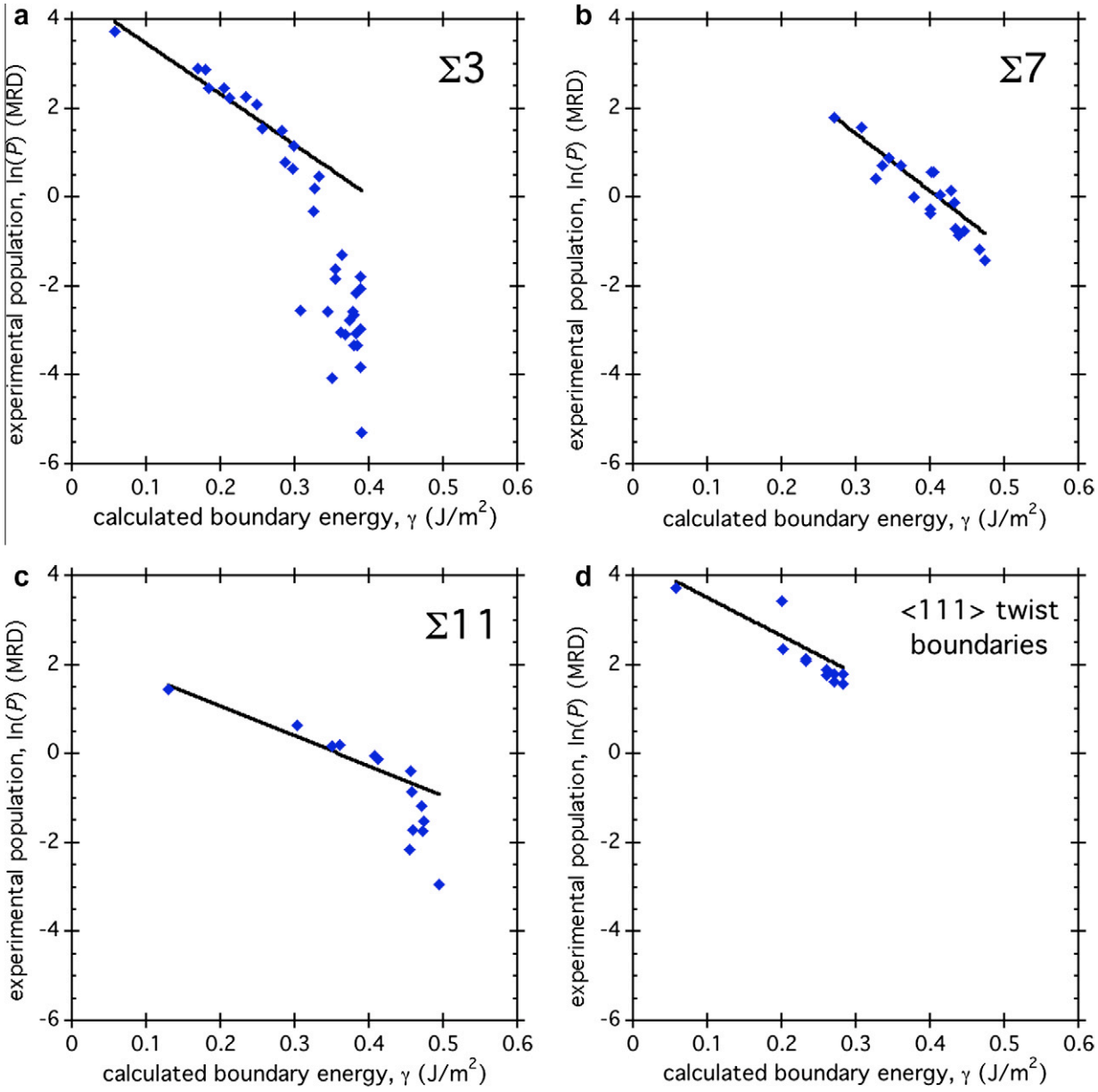

Fig. 3. The relationship between experimental GBCD and calculated grain boundary energy for special boundary types in Al. Population-weighted linear fits are shown as solid lines. (a) Σ3 boundaries show a strong correlation between GBCD and energy for high population boundaries ($P > 1$). (b) Σ7 boundaries show a strong correlation over the population range. (c) Σ11 boundaries show a strong correlation for high and mid-population boundaries ($P > -1$). (d) ⟨1 1 1⟩ twist boundaries are all of high population, and show a strong correlation between measured GBCD and calculated energy.

$R_W = 0.86$), as shown in Fig. 3c. Again, the 50.6°[1 1 1] (1 1 1) symmetric twist boundary is an outlier, due to overlap with the Σ3 population.

While ⟨1 1 1⟩ boundary planes are favored in Ni [44], twinning so dominates the Ni microstructures that all other boundary types, including ⟨1 1 1⟩ boundaries, are marginalized. However, MD simulations indicate that ⟨1 1 1⟩ twist boundaries are relatively lower in energy in Al than in Ni [40]. This would suggest ⟨1 1 1⟩ twist boundaries should be more plentiful in Al than in Ni, in agreement with experimental observations.

3.5. Comparing GBCDs in Ni and Al

Computer simulations of identical grain boundaries in different fcc metals indicate that, for a given grain boundary crystallography, the energy scales with the shear modulus [40]. Using GBCD data for Ni and Al, we can examine whether the energy scaling observed in simulations is reflected in boundary population measurements. Because of differences in the amounts of data, the GBCDs of Ni and Al were computed at different resolutions. In any discrete system, the maximum population in MRD is equal to

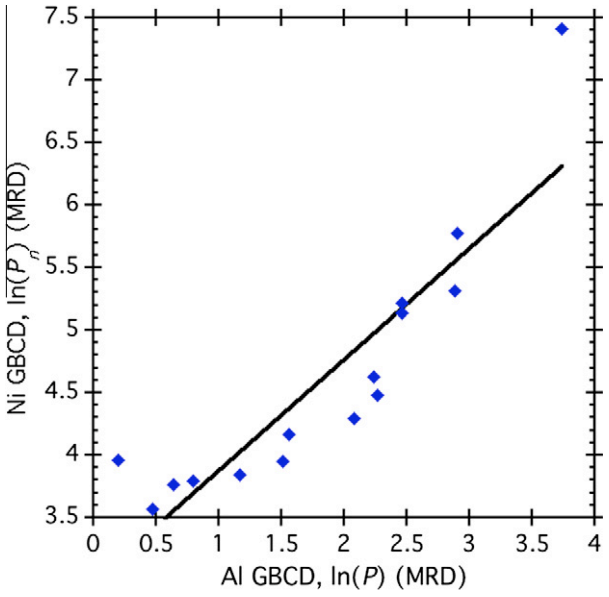

Fig. 4. The relationship between experimental GBCDs in Ni and Al for high population boundary types ($P_n > 1$ MRD in Ni and $P > 1$ MRD in Al). The population criteria limit the boundaries to Σ3 types. The Ni and Al GBCDs are positively correlated, with the solid line indicating an unweighted linear fit, as suggested by simulations.

the number of bins, so the maximal population values differ in Ni and Al. Therefore, in all direct comparisons of the two distributions, the Ni populations will be normalized by a factor of 2.73 (i.e. $P_n(Ni) = P(Ni)/2.73$), which is the ratio of the number of bins in the Ni GBCD to the number in the Al GBCD. This scaling underestimates the populations of the low P boundaries; however, in comparing Ni and Al we will consider only high P boundaries.

Fig. 4 shows population data for the surveyed boundaries that are statistically meaningful in both Ni and Al (i.e. $P_n > 1$ MRD in Ni and $P > 1$ MRD in Al). The population criteria limit the boundaries to Σ3 types. However, for this limited boundary set, the Ni and Al GBCDs are positively correlated, and the scaling is plausibly represented by an unweighted linear fit ($R_U = 0.90$), as predicted by simulations. The slope of the best-fit line ($m = 0.9$) is not related to the ratio of shear moduli (the Voight average shear modulus ratio $\mu(\text{Ni}):\mu(\text{Al}) = 3.5$). Since the scaling factor between ln(P) and absolute boundary energy is not known, it is not surprising that the shear modulus ratio is not directly recovered. Nonetheless, the good agreement between relative populations in Ni and Al corroborates the scaling observed in simulations.

4. Conclusions

While direct comparisons between measured and calculated grain boundary energies have been performed [33], extracting energy data from stereological observations requires careful serial sectioning and extensive numerical post-processing. Alternately, the grain boundary character distribution (GBCD) is a direct measurement that can be determined from a single planar section. Since both theory and experiments suggest that the GBCD is inversely related to the grain boundary energy distribution (GBED), we tested whether the experimental GBCD could be used to validate the computed GBED by comparing measured GBCD data to calculated energies for 388 grain boundaries in Al. Analysis of the results suggest several conclusions:

1. For boundaries with a statistically reliable number of observations, the GBCD correlates very well with calculated grain boundary energy. Specifically, $\ln(P) \propto \gamma$, where P is the boundary population and γ is the grain boundary free energy.
2. For infrequently observed boundaries, the computed grain boundary energy may be more accurate than estimates based on the measured GBCD.
3. Excellent agreement between the GBCD and energy for high population Σ3 boundaries corroborates previous observations in Ni [33].
4. The GBCD correlates well with energy for other boundary types that have not been validated previously, including Σ7, Σ11 and ⟨1 1 1⟩ twist boundaries. Both qualitative and quantitative trends seen in simulations are reproduced in experiments.
5. Because Al lacks the extensive twinning that skews the GBCD and disrupts the general grain boundary network in Ni, the Al GBCD provides a good estimate of energy for more boundary types than is possible in Ni.
6. For high population boundary types, the Ni and Al GBCDs are positively correlated, in agreement with simulation predictions.

Overall, we found the GBCD to be a useful metric for validating grain boundary energy calculations. By combining GBCD measurements with simulation results, we obtain the first large-scale, validated grain boundary data set for both low and high stacking fault energy metals.

Acknowledgements

Sandia National Laboratories is a multi-program laboratory managed and operated by Sandia Corporation, a wholly owned subsidiary of Lockheed Martin Corporation, for the US Department of Energy's National Nuclear Security Administration under contract DE-AC04-94AL85000. We acknowledge support from the Department of Energy, Office of Basic Energy Sciences both through the core program and through the Computational Materials Science Network program. The work at CMU was primarily supported by the MRSEC program of the National Science Foundation under Award Number DMR-0520425.

References

[1] Sutton AP. Int Metals Rev 1984;29:377–402.
[2] Sutton AP, Balluffi RW. Acta Metall 1987;35:2177–201.

[3] Sutton AP, Vitek V. Philos Trans Roy Soc Lond Ser A, Math Phys Sci 1983;309:1–36.
[4] Wang G-J, Vitek V. Acta Metall 1986;34:951–60.
[5] Wolf D, Yip S. Materials interfaces: atomic-level structure and properties. London: Chapman & Hall; 1992.
[6] Olmsted D, Foiles SM, Holm EA. Acta Mater 2009;57:3694–703.
[7] Amouyal Y, Rabkin E. Acta Mater 2007;55:6681–9.
[8] Amouyal Y, Rabkin E, Mishin Y. Acta Mater 2005;53:3795–805.
[9] Barmak K, Kim J, Kim CS, Archibald WE, Rohrer GS, Rollett AD, et al. Scripta Mater 2006;54:1059–63.
[10] Chan SW, Balluffi RW. Acta Metall 1985;33:1113–9.
[11] Chan SW, Balluffi RW. Acta Metall 1986;34:2191–9.
[12] Gjostein NA, Rhines FN. Acta Metall 1959;7:319–30.
[13] Hasson G, Boos J-Y, Herbeuval I, Biscondi M, Goux C. Surf Sci 1972;31:115–37.
[14] Hasson GC, Goux C. Scr Metall 1971;5:889–94.
[15] McLean M. J Mater Sci 1973;8:571–6.
[16] Miura H, Kato M, Mori T. J Mater Sci Lett 1994;13:46–8.
[17] Read WT, Shockley W. Phys Rev 1950;78:275–89.
[18] Schmelzle R, Muschik T, Gust W, Predel B. Scr Metall Mater 1991;25:1981–6.
[19] Skidmore T, Buchheit RG, Juhas MC. Scripta Mater 2004;50:873–7.
[20] Wolf U, Ernst F, Muschik T, Finnis MW, Fischmeister HF. Philos Mag A-Phys Condens Matter Struct Defects Mech Prop 1992;66:991–1016.
[21] Straumal BB, Polyakov SA, Bischoff E, Gust W, Mittemeijer EJ. Interface Sci 2001;9:287–92.
[22] Adams BL, Ta'asan S, Kinderlehrer D, Livshits I, Mason DE, Wu C-T, et al. Interface Sci 1999;7:321–38.
[23] Kim C-S, Hu Y, Rohrer GS, Randle V. Scripta Mater 2005;52:633–7.
[24] Kim C-S, Rollett AD, Rohrer GS. Scripta Mater 2006;54:1005–9.
[25] Li J, Dillon SJ, Rohrer GS. Acta Mater 2009;57:4304–11.
[26] Morawiec A. Acta Mater 2000;48:3525–32.
[27] Rohrer GS, Li J, Lee S, Rollett AD, Groeber M, Uchic MD. Mater Sci Technol 2010;26:661–9.
[28] Rohrer GS, Saylor DM, Dasher BE, Adams BL, Rollett AD, Wynblatt P. Zeitschrift für Matallkunde 2004;95:197–214.
[29] Saylor DM, El Dasher BS, Rollett AD, Rohrer GS. Acta Mater 2004;52:3649–55.
[30] Saylor DM, El-Dasher BS, Adams BL, Rohrer GS. Metall Mater Trans A-Phys Metall Mater Sci 2004;35A:1981–9.
[31] Saylor DM, Morawiec A, Rohrer GS. Acta Mater 2003;51:3675–86.
[32] Saylor DM, Morawiec A, Rohrer GS. Acta Mater 2003;51:3663–74.
[33] Rohrer GS, Holm EA, Rollett AD, Foiles SM, Li J, Olmsted DL. Acta Mater 2010;58:5063–9.
[34] Daw MS, Foiles S, Baskes MI. Mater Sci Reports 1993;9:251–310.
[35] Ercolessi F, Adams JB. Europhys Lett 1994;26:583.
[36] Brandon DG. Acta Metall 1966;14:1479–84.
[37] Gruber J, Miller HM, Hoffmann TD, Rohrer GS, Rollett AD. Acta Mater 2009;57:6102–12.
[38] Gruber J, Rollett AD, Rohrer GS. Acta Mater 2010;58:14–9.
[39] Rohrer GS. Ann Rev Mater Res 2005;35:99–126.
[40] Holm E, Olmsted D, Foiles S. Scripta Mater 2010;63:905–8.
[41] Schmidt C, Finnis MW, Ernst F, Vitek V. Philos Mag A 1998;77:1161–84.
[42] Liebmann B, Lucke K, Graham CD, Cahn RW, Dunn CG. Trans Am Inst Min Metall Eng 1956;206:1413–6.
[43] Molodov DA, Czubayko U, Gottstein G, Shvindlerman LS. Scripta Metall et Mater 1995;32:529–34.
[44] Randle V, Rohrer GS, Miller HM, Coleman M, Owen GT. Acta Mater 2008;56:2363–73.